aerospace

MDPI

Article

Optimization of Low-Altitude Vertiport Network Topology Resilience

Hua Xie [1,2,3], Ziyuan Zhu [1,2], Jianan Yin [2,3,4,*], Yuhang Wu [1,2], Long Zhou [4,5] and Qingchun Wu [3]

[1] College of General Aviation and Flight, Nanjing University of Aeronautics and Astronautics, Changzhou 213300, China; xiehua@nuaa.edu.cn (H.X.); zhuziyuan@nuaa.edu.cn (Z.Z.); wu_yuhang@nuaa.edu.cn (Y.W.)
[2] State Key Laboratory of Air Traffic Management System, Nanjing 211106, China
[3] Shenzhen Research Institute, Nanjing University of Aeronautics and Astronautics, Shenzhen 518110, China; wqc520@nuaa.edu.cn
[4] College of Civil Aviation, Nanjing University of Aeronautics and Astronautics, Nanjing 211106, China; zhoulongzwzl@163.com
[5] Nanjing Intelligent Aviation Research Institute Co., Ltd., Nanjing 210014, China
* Correspondence: j.yin@nuaa.edu.cn

Abstract

This study investigates the construction of a topological network for resilient low-altitude vertiports. Addressing the issue of excessive network redundancy often caused by maximizing algebraic connectivity in traditional topology optimization problems, we employ algebraic connectivity—a key spectral metric—as a measure of network topology resilience. The objective function employs normalized algebraic connectivity that simultaneously considers total network distance, achieving an effective trade-off between global fault tolerance and construction costs at the model level. To address this challenging combinatorial optimization problem, the Gray Wolf Optimizer (GWO) algorithm is mechanistically enhanced. Experiments demonstrate that the proposed method achieves superior performance in key metrics such as objective function value and total network distance, significantly enhancing network resilience while controlling construction costs. For the optimized network topology solutions, simulations of six failure modes for nodes and edges analyze the response characteristics of the vertiport network's maximum connected subgraph proportion and global efficiency during the gradual removal of nodes and edges. Results demonstrate that the designed vertiport topology network exhibits robust resilience. It maintains high connectivity and global efficiency under both random attacks and degree-based targeted node attacks, showcasing strong engineering applicability.

Keywords: vertiport; topological networks; algebraic connectivity; gray wolf optimization algorithm; network resilience

Check for updates

Academic Editor: Michael Schultz

Received: 4 March 2026
Revised: 5 April 2026
Accepted: 11 April 2026
Published: 15 April 2026

Copyright: © 2026 by the authors. Licensee MDPI, Basel, Switzerland. This article is an open access article distributed under the terms and conditions of the Creative Commons Attribution (CC BY) license.

1. Introduction

In recent years, rapid urbanization and increasingly dense urban spatial structures have placed significant pressure on traditional urban transport systems. These systems, which primarily rely on surface transport, are now facing a series of structural bottlenecks. These include declining travel efficiency, worsening traffic congestion, and inadequate emergency response capabilities [1]. Against this backdrop, novel transport modes tailored for low-altitude airspace have garnered increasing attention from both academic and engineering circles. Low-altitude aircraft, exemplified by electric vertical take-off and

landing (eVTOL) vehicles, are regarded as a key technological pathway for alleviating urban traffic congestion and expanding three-dimensional transport capacity within cities. This is due to their reduced reliance on runways, enhanced operational flexibility, and suitability for short-distance, high-frequency operations.

With the continuous maturation of propulsion systems, battery technology, flight control, and airspace management capabilities, low-altitude flight operations have evolved beyond isolated trials or demonstration runs, progressively advancing towards systematic and networked integration. Within this process, low-altitude vertiports serve as critical infrastructure nodes within the low-altitude transport system. Their spatial layout and interconnection methods directly determine the operational efficiency, service coverage capacity, and overall safety level of the low-altitude transport network. Compared with traditional aviation hub systems, low-altitude vertiports are more numerous and spatially dispersed. As a result, they exhibit typical characteristics of complex network structures. This makes it difficult for planning based solely on empirical rules or localized optimal strategies to meet system-level operational requirements.

From a systems engineering perspective, a low-altitude vertiport network must not only exhibit high accessibility and operational efficiency during normal conditions but also maintain core functionality when confronted with node failures, segment disruptions, or sudden incident impacts. Such disturbances may stem from multiple factors, including extreme weather, equipment malfunctions, temporary airspace restrictions, and sudden public safety incidents. Should the network structure lack sufficient inherent robustness, localized failures can readily propagate through the topology, triggering chain reactions that lead to widespread operational degradation or even systemic paralysis. Consequently, establishing low-altitude vertiport networks with 'intrinsic resilience' during the planning phase has become a critical prerequisite for enabling the large-scale operation of low-altitude air traffic.

To systematically address the optimization of low-altitude vertiport network topology resilience, this study employs a progressive chapter design. Theoretically, it innovates a resilience optimization paradigm for low-altitude networks; methodologically, it provides scalable solution algorithms and empirical validation. Section 2 provides a systematic review of existing studies on the resilience analysis and optimization of low-altitude complex networks. Section 3 addresses the core requirement of balancing resilience and economic feasibility in low-altitude vertiport networks. Drawing on graph theory, it introduces algebraic connectivity as a resilience metric and proposes a normalized algebraic connectivity objective function. The model is relaxed using semi-definite programming (SDP) to reduce computational complexity. Section 4 introduces a mechanism-based enhancement of the GWO algorithm for solving the maximum algebraic connectivity problem. Section 5 systematically validates the proposed model and algorithm using 33 low-altitude vertiports in Shenzhen as empirical subjects. Sensitivity analysis determines the reasonable range for the maximum node degree constraint, while comparing the performance of different algorithms in solving the problem. Additionally, the resilience of the network under five failure modes is simulated. Section 6 summarizes the theoretical contributions and practical value of this work, while identifying future research directions for studying the resilience of low-altitude vertiport networks.

2. Literature Review

Research has demonstrated that the topological structure of infrastructure networks exerts a decisive influence on their resilience. Different topological characteristics—such as node distribution, connection redundancy, and inter-layer dependencies—can significantly alter a network's susceptibility to random failures and malicious attacks [2]. In domains

such as transport networks, power grids and telecommunications networks, rational topological design can significantly enhance a system's resilience against random failures and deliberate attacks [3].

This study investigates the construction of a topological network for resilient low-altitude vertiports. Traditional topology optimization methods that maximize algebraic connectivity often led to excessive network redundancy. To address this issue, algebraic connectivity is adopted in this study as a key measure of network resilience. The objective function employs normalized algebraic connectivity that simultaneously considers total network distance. A semidefinite programming approach relaxes the model, achieving an effective trade-off between global fault tolerance and construction costs at the model level. To address this challenging combinatorial optimization problem, the Grey Wolf Optimizer algorithm is mechanistically enhanced. Experimental results show that the proposed method outperforms benchmark approaches in key metrics, including objective function value and total network distance. It also enhances network resilience while effectively controlling construction costs. For the optimized network topology solutions, simulations of five failure modes for nodes and edges analyze the response characteristics of the vertiport network's maximum connected subgraph proportion and global efficiency during the gradual removal of nodes and edges. Results demonstrate that the designed vertiport topology network exhibits robust resilience. It maintains high connectivity and global efficiency under both random attacks and degree-based targeted node attacks, showcasing strong engineering applicability.

The resilience of transport networks directly impacts social stability, economic development, and public safety. This critical importance stems from modern society's profound reliance on the connectivity and timeliness sustained by transportation. Presently, scholars across various disciplines have conducted extensive research on transport networks. In road traffic research, resilience is defined as a road segment's ability to withstand and recover from traffic flow disturbances [4]. Research on the resilience of the U.S. Strategic Highway Network infrastructure system has found that the network exhibits strong structural robustness. The highway network is better able to withstand disruptions and maintain overall functionality, whereas the railway network demonstrates greater connectivity vulnerability, particularly under targeted attack scenarios where functional loss is more likely to occur [5]. Empirical analysis of Hong Kong's public transport network demonstrates that connectivity between multimodal systems enhances overall resilience against random disruptions or targeted attacks. In aviation networks, studies have considered the impact of different altitude layers on airspace efficiency and evaluate the system's survivability [6]. Analysis of the complex network topology characteristics of integrated air-rail networks reveals that while the integrated network enhances efficiency, it also creates a high degree of dependency on hub nodes, making the network vulnerable to disruptions [7].

As low-altitude air traffic systems evolve toward networked and high-density operations, decentralized airspace traffic management has gained increasing attention. In this context, the method proposed by Veytia et al. [8] provides valuable insights into the operational mechanisms of low-altitude route networks. They abstract urban low-altitude airspace as a route network within a constrained urban airspace and introduce dynamic control strategies based on traffic complexity, achieving self-organizing optimization of traffic flow without centralized control. By reducing traffic complexity, they effectively mitigate the risks of potential conflicts and congestion [8]. Research on the survivability of low-altitude vertiport networks. Clarke et al. investigated resilience control strategies for Urban Air Mobility (UAM) systems under Distributed Denial of Service (DDoS) cyber-attacks, introducing the K-cut problem from graph theory to quantify node vulnerability and proposing a distributed control framework that integrates vulnerability assessment,

self-reconfiguration, and distributed optimization to adaptively adjust the behavior of unmanned aerial vehicles [9]. Ma's team conducted a series of studies on the resilience of urban multimodal transportation networks, proposing a constraint-based clustering model with neighborhood search to determine vertiport locations and developing a cascading-failure resilience assessment framework grounded in percolation theory; through a case study in Beijing, they evaluated network performance in terms of structural connectivity and demand fulfillment and demonstrated that integrating metro systems with urban air mobility networks improves connectivity by offering alternative routes, thereby enhancing overall urban multi-modal transportation (UMT) network resilience by approximately 9–11% [10,11]. Zhang et al. proposed an optimization framework for vertiport networks incorporating connectivity constraints with the dual objectives of minimizing transportation and construction costs, and developed a hybrid genetic algorithm integrating Minimum Spanning Tree (MST) and greedy initialization to address problems of varying scales, achieving resilience performance comparable to benchmark solutions while significantly reducing computational time and thus providing effective decision support for UAM planning in complex urban environments [12]. Song et al. proposed a network topology–based approach for vertiport location allocation, emphasizing that overall system performance is fundamentally determined by global structural characteristics rather than traditional local optimization, and analyzed how different layout strategies influence network efficiency and structural properties through comprehensive network metric evaluation [13]. Fung developed a resilience-oriented design methodology for UAM systems that uses large-scale simulations of off-nominal disruptions—such as vertiport closures and airspace management failures—to diagnose operational vulnerabilities and extract design heuristics from system responses, thereby offering guidance for resilience evaluation and infrastructure planning in complex real-world UAM environments [14]. Liu et al. considered spatial continuity and accessibility in planning low-altitude transportation networks at the urban agglomeration scale, and emphasized that network connectivity and redundancy are crucial for ensuring operational safety in future systems [15]. Cheng et al. [16] considered the effects of wind speed and rainfall on low-altitude logistics networks. Taking a low-altitude logistics network constructed based on UAV takeoff and landing sites in Shenzhen as a case study, they conducted a comparative analysis of the network robustness under different node removal strategies and proposed optimization recommendations for enhancing network resilience [16].

By abstracting the low-altitude vertiport system as a topological network and applying key metrics from complex network and spectral graph theory, this approach effectively reveals its overall structural characteristics, combining theoretical depth with engineering feasibility. Current methods for optimizing network resilience primarily focus on enhancing topological connectivity and redundancy, often employing strategies like dynamic control or layout optimization to improve survivability under disturbances. While characterizing the intrinsic relationship between connectivity and resilience from a global perspective helps identify critical connections that significantly impact system robustness during planning—providing valuable theoretical and methodological support for network construction—a fundamental challenge remains. The construction of vertiports and the establishment of flight segments involve high economic costs and stringent airspace constraints, making it impractical to pursue robustness solely by adding redundant connections. Therefore, planning methodologies must achieve a more refined trade-off between network performance and construction costs. This underscores the urgent need for a new paradigm in topological optimization, one that can effectively and fundamentally balance resilience performance with construction economy.

3. Model Construction

The efficient and stable operation of urban air mobility (UAM) systems heavily relies on the reliability of their underlying infrastructure networks. As the operational foundation for eVTOL aircraft, the topology of the low-altitude vertiport network directly determines traffic flow organization efficiency and system survivability. From the perspective of the UAM planning framework, network planning can be divided into three levels: strategic-level topological network planning, tactical-level route network design, and operational-level flight path planning and obstacle avoidance. This chapter focuses on the preliminary planning of transport network topology at the strategic level. It aims to address connectivity between planning nodes and construct a foundational network backbone with inherent resilience. This represents a macro-level planning challenge and provides a stable basis for subsequent UAM operations. A well-designed landing site network topology should possess the following characteristics:

1. Intrinsic Resilience;

When partial node or edge failures occur due to equipment malfunctions, adverse weather, airspace restrictions, or other unforeseen events, the network must maintain connectivity among remaining components to prevent localized failures from causing system-wide collapse.

2. Economic Feasibility.

While establishing direct connections between every pair of landing sites (i.e., creating a fully connected network) would achieve exceptional resilience, the resulting construction investment and operational costs would be prohibitively high. Therefore, an optimal balance must be sought between network performance and construction expenses.

Therefore, the core research question of this paper can be defined as constructing a network with the highest possible resilience while minimizing the total network distance, ensuring it maintains robust connectivity even when faced with localized failures.

To highlight the impact of network topology on system resilience, this study abstracts the real system while preserving the core research problem. Non-critical factors are excluded, and the following assumptions are introduced:

(1) Since the horizontal spacing required for connectivity between vertiports far exceeds their vertical displacement, the effects of terrain undulations and vertical elevation changes on network topology are neglected; only the two-dimensional connected network planning problem is considered;

(2) Assuming that eVTOL aircraft operate only within approved airspace over land and inland water bodies; this does not include exempted routes crossing restricted airspace, nor does it include transoceanic or interregional flights;

(3) All edges between vertiports in the network are assumed to be bidirectional, undirected edges with identical communication and navigation support capabilities;

(4) All vertiports within the network are assumed to be integrated into a single connected network, disregarding isolated nodes or subgraphs;

(5) Nodes and edges are assumed to exist only in two states: "fully operational" or "completely failed," without considering performance degradation scenarios.

In the theoretical framework of graph theory, the Laplacian matrix L is mathematically defined as the difference between the degree matrix D_k and the adjacency matrix A:

$$L = D_k - A \tag{1}$$

$$L_{ij} = \begin{cases} \deg(v_i) & , i = j \\ -1 & , z_{ij} = 1 \\ 0 & , \text{other} \end{cases} \tag{2}$$

where v_i represents the i-th node in the network; z_{ij} is a binary variable that indicates whether v_i and v_j are connected.

Let λ_i denote the eigenvalues of the Laplace matrix. Sort the eigenvectors $0 = \lambda_1 \leq \lambda_2 \leq \ldots \leq \lambda_N$ such that the smallest eigenvalue is 0, while the next smallest eigenvalue λ_2 is referred to as the algebraic connectivity of the graph. If the algebraic connectivity is 0, it indicates that at least one pair of nodes in the network cannot be connected via either a direct or indirect path. A higher algebraic connectivity value signifies that more edges must be removed to partition the graph into disconnected components, thereby indicating greater global resilience of the network.

Typically, network topology optimization problems aim to maximize algebraic connectivity λ_2. However, pursuing higher values tends to transform the graph into a dense, fully connected network, imposing greater burdens on the infrastructure. Due to the vast difference in magnitude between λ_2 and network distance, the weighted Laplace method—commonly used in complex network problems—faces difficulties in determining appropriate weights. To strike a balance between global resilience and network cost, this study adopts normalized algebraic connectivity F, defined with network distance as the denominator, as the objective function. F represents the gain in global network resilience achieved per unit of construction cost. As a dimensionless metric that accounts for marginal benefits, this objective resolves the weight selection problem while ensuring that, during the solution process, the algorithm will inherently prioritize the construction of key connections that contribute significantly to global resilience at relatively low cost. Consequently, it selects the topological network structure with the highest resilience payoff while taking cost into account. The calculation method for normalized algebraic connectivity is shown in Equation:

$$\begin{aligned} & F = \max \frac{\lambda_2(G)}{\sum\limits_{i<j} D_{ij} z_{ij}} \\ & s.t. \quad G = (V, E') \\ & \qquad E' = \left\{ (i,j) \middle| z_{ij} = 1 \right\}, E' \subseteq E \\ & \qquad z_{ij} \in \{0,1\} \\ & \qquad \forall (i,j) \in E' \end{aligned} \tag{3}$$

where D_{ij} represents the flight distance between nodes v_i and v_j; z_{ij} denotes the decision variable used to determine whether nodes v_i and v_j are connected. The larger the value of F, the better the cost-effectiveness and resilience of the network topology.

Since λ_2 is a nonlinear eigenvalue, it is difficult to solve exactly when the problem involves matrix inequality constraints. Consequently, in network optimization problems aimed at maximizing algebraic connectivity, it is often difficult to assess the gap between the optimality of a design and the performance limit. This section reduces the solution difficulty by relaxing λ_2. By extending the binary decision variable z_{ij} to a continuous variable z'_{ij} on the interval $[0,\ 1]$, the relaxed formulation of Equation (3) becomes:

$$\begin{aligned} & F = \max \xi(G) = \max \frac{\lambda_2(G)}{\sum\limits_{i<j} D_{ij} z'_{ij}} \\ & s.t. \quad L(z') = \sum_{i<j} z'_{ij} E_{ij} \\ & \qquad z'_{ij} \in [0,1] \\ & \qquad \forall (i,j) \in E' \end{aligned} \tag{4}$$

where E_{ij} is the Laplace matrix corresponding to the edge (i,j).

Since Equation (4) possesses a larger feasible set than Equation (3), it is possible to find a maximum lower bound s such that all eigenvalues of the matrix exceed s except for the smallest zero eigenvalue. To address the non-convexity issue arising from the fractional structure in the original objective function, an auxiliary variable $t > 0$ is introduced to perform a Charnes-Cooper transformation. Setting $w_{ij} = t \cdot z'_{ij}$ maps the original problem to a higher-dimensional convex space. After transformation, the problem can be reformulated as an equivalent relaxed SDP problem [17]. The complete relaxed model is formulated as follows:

$$F = \max s \tag{5}$$

$$s.t.\ L(w) + \frac{t}{N}\mathbf{1}\mathbf{1}^T \succeq s I_n \tag{6}$$

$$\sum_{i<j} D_{ij} w_{ij} = 1 \tag{7}$$

$$w_{ij} \in [0, t] \tag{8}$$

$$1 \leq \sum_{v_j \in V} z_{ij}\ \forall v_i \in V \tag{9}$$

$$S \subset V,\ S \neq \varnothing,\ S \neq V \tag{10}$$

$$\sum_{v_j \in V, j \neq i} z_{ij} \leq K\ \forall v_i \in V \tag{11}$$

$$\widetilde{D}_{ij} \cdot z_{ij} \leq D_{\max}\ \forall (i,j) \in E' \tag{12}$$

$$z_{ij} \cdot \mathbb{I}(\mathrm{int}(i,j) \cap O_q \neq \varnothing) = 0, \quad \forall q \in \{1, \ldots, Q\}, (i,j) \in E' \tag{13}$$

$$z_{ij} = \begin{cases} 1\text{ , if } v_i \text{ and } v_j \text{ are connected} \\ 0\text{ , other} \end{cases} \quad \forall v_i, v_j \in V, i \neq j \tag{14}$$

where I_n denotes the identity matrix, $\mathbf{1}$ represents the all-ones matrix, $D_{\max}$ signifies the aircraft's maximum operational range constraint; $\mathcal{O}$ is the set of all no-fly zones; Q indicates the number of no-fly zones; $\mathbb{I}(\cdot)$ is a characteristic function defined such that when a point inside a line segment intersects a no-fly zone, $z_{ij} = 0$.

The objective function (5) refers to the objective function under SDP; Constraints (6) denotes the spectral constraint under the SDP; Constraints (7) specifies the normalization constraint; Constraints (8) defines the range of auxiliary variables; Constraints (9) ensures each vertiport connects to at least one edge; Constraints (10) guarantees the generated graph $G = (V, E')$ is connected, i.e., there is no non-empty subset S of the true nodes such that S is completely disconnected from the rest of the graph. Constraints (11) represents the maximum node degree constraint. Given the limited airspace resources and landing platforms at each low-altitude vertiport, this constrains each node's degree value to not exceed a maximum processing capacity. Constraints (12) ensures that the distance between connected vertiports meets the maximum operational range requirement, guaranteeing that the connectivity between sites is operationally feasible. Constraints (13) prohibits edges from crossing no-fly zones. Equation (14) defines the variable domain.

4. Method

Since the problem of maximizing algebraic connectivity is NP-hard [18], there are currently no efficient exact solution methods for optimizing algebraic connectivity in large-scale networks. Therefore, this paper employs a meta-heuristic algorithm to address this problem.

4.1. Basic Gray Wolf Optimization Algorithm

The Gray Wolf Optimizer Algorithm (GWO) is a swarm intelligence optimization algorithm that simulates the social hierarchy and cooperative hunting behavior of gray wolf packs, dividing individuals into four social ranks $\alpha, \beta, \delta, \omega$. Each equivalent gray wolf individual assumes different responsibilities, as shown in Table 1.

Table 1. Mapping of Social Hierarchy and Algorithms in GWO.

Rank	Role	Purpose	Optimization Meaning
α	Optimal Solution	The best candidate solution in the current population	Guide search direction, reflecting the current optimal solution
β	Suboptimal Solution	Assist α in decision-making	Avoid getting stuck in local optima
δ	Third-best Solution	Participate in guided search	Enhance population diversity
ω	Other individuals	Guided candidate solutions	Learn from α, β, δ and update your own position.

The gray wolf hunting process consists of the following three stages:

(1) Encircling the prey: During the encirclement phase, the wolf pack dynamically adjusts its spatial positioning based on the prey's real-time location, ensuring the search gradually concentrates on the potentially optimal area.

(2) Cooperative hunting: Gray wolf hunting behavior primarily relies on the guidance of wolves α, β and δ, using the three optimal solutions within the population to direct position updates for other individuals.

(3) Pursuing prey: When the prey ceases movement, the pursuit phase commences. The GWO algorithm simulates this closing-in process by progressively reducing the value of $\vec{a}$ during iterations.

4.2. Improved GWO Algorithm

1. Circle Chaos Mapping Initialization;

In standard gray wolf optimization algorithms, the initial population is typically generated randomly, which may result in uneven population distribution and affect the algorithm's convergence efficiency. Chaotic mappings can produce more uniformly distributed initial populations. Such methods provide a solid foundation for global search and are widely applied in population initialization optimization for intelligent algorithms. Commonly used chaotic sequences include the Logistic map, Tent map, and Circle map. However, the Logistic map exhibits a Chebyshev distribution, tending to values between [0, 0.1] and [0.9, 1], resulting in uneven distribution; The Tent map yields a uniform distribution, but after a certain number of iterations, the chaotic sequence may converge to a fixed point or begin repeating cyclically, losing its chaotic properties. Therefore, this study employs the Circle map for population initialization, which offers uniform distribution while being more stable than the Tent map. The distribution map of Circle Chaos Mapping is shown in Figure 1.

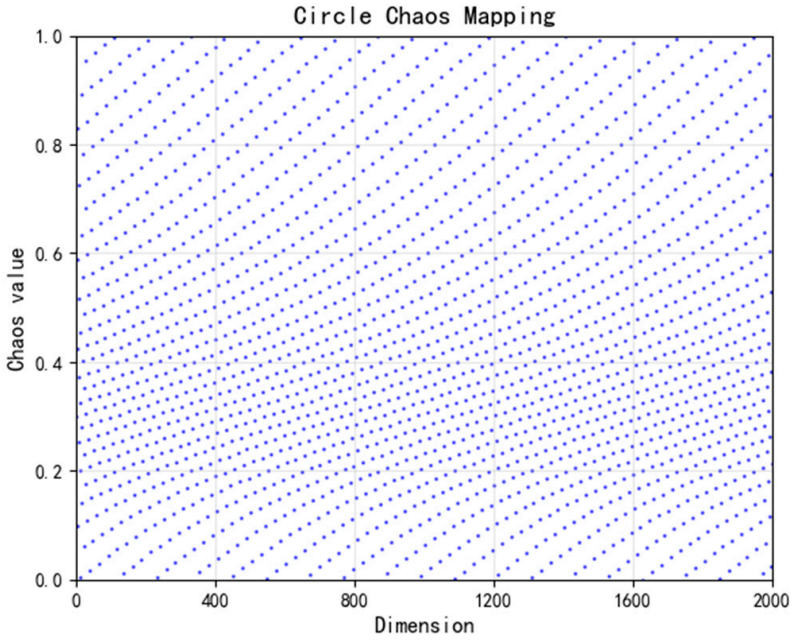


Figure 1. Distribution of the Circle Chaos Map.

2. Nonlinear Convergence Factor;

The values assigned to coefficient parameters in the GWO algorithm significantly influence its search behavior. The baseline GWO algorithm sets the convergence factor $\vec{a}$ to decrease linearly from 2 to 0 during iterations, which often fails to align with the actual optimization process. During the early stages of iteration, the steep decline rate of convergence factor $\vec{a}$ may prevent the algorithm from thoroughly exploring the solution space. Therefore, this study introduces a nonlinear convergence factor $\vec{a}'$, expressed as follows:

$$\vec{a}' = 2 - 2\left(\frac{T}{\max_Iter}\right)^4 \tag{15}$$

The trend curve showing the diminishing trend of the improved nonlinear convergence factor $\vec{a}'$ with the number of iterations is depicted in Figure 2.

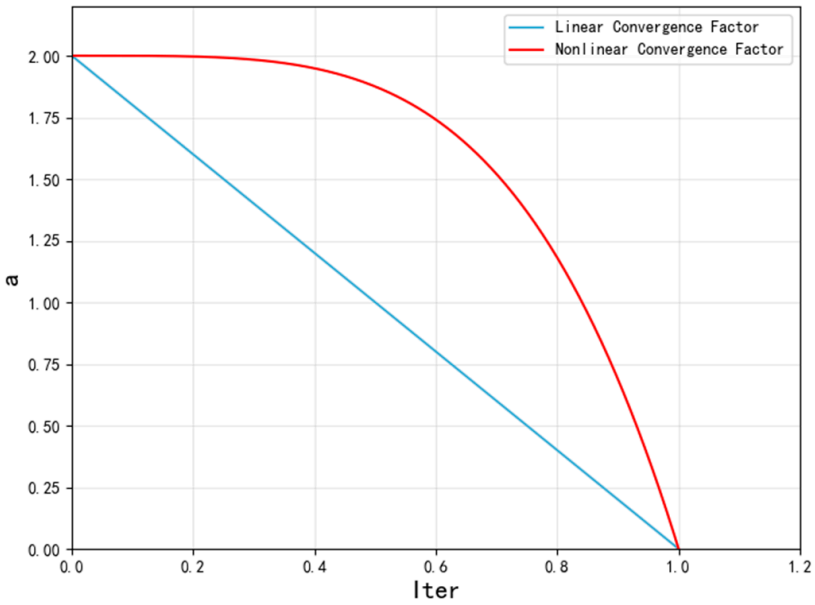


Figure 2. Comparison of Nonlinear Convergence Factors and Linear Convergence Factors.

3. Dynamic Reflection Backward Learning Strategy.

Due to the GWO algorithm's excessive reliance on the position of Alpha Wolf, it lacks an effective escape mechanism when trapped in local optima. Therefore, this study introduces a dynamic refraction-based reverse learning strategy into the population update process of GWO to enhance the algorithm's ability to overcome local optimization. Refraction-based reverse learning is an intelligent optimization strategy inspired by optical refraction principles. It generates new solutions by simulating light refraction at interfaces between different media. Compared to conventional back-propagation methods, when an optimization algorithm becomes trapped in a local optimum, standard back-propagation merely maps the solution to another symmetric region. In contrast, refraction back-propagation, due to its variable search direction, has a higher probability of escaping the current predicament. It guides the population to continue moving toward promising regions, thereby reactivating the algorithm's search capability [19].

In Figure 3, $X_{\max}$ and $X_{\min}$ represent the upper and lower bounds of the problem, respectively. A^* denotes the landing point of A after refraction. X, X^*, h, and h^* represent the projections of A and A^* onto the x-axis and y-axis, respectively. The expression for the inverse solution $X^*(T)$ of $X(T)$ and the principle for preserving the solution are as follows:

$$X^*(T) = \frac{X_{\max} - X_{\min}}{2} + \frac{X_{\max} + X_{\min}}{2\eta} - \frac{X(T)}{\eta} \tag{16}$$

$$\overline{X}(T) = \begin{cases} X^*(T)\ , \ fitness(X^*(T)) > fitness(X(T)) \\ X(T)\ \ , \ other \end{cases} \tag{17}$$

where $\eta = h/h^*$ represents the refractive index parameter; $\overline{X}(T)$ denotes the optimal solution retained after dynamic reflection backward learning; $fitness(\cdot)$ is the fitness evaluation function. Typically, η is a constant. However, since refractive regions may also become trapped in local optima, η is set as a dynamic value that adapts during iterations, expressed as shown in the formula:

$$\eta = \left(1 + \sqrt{\frac{T}{\max_Iter}}\right)^{10} \tag{18}$$

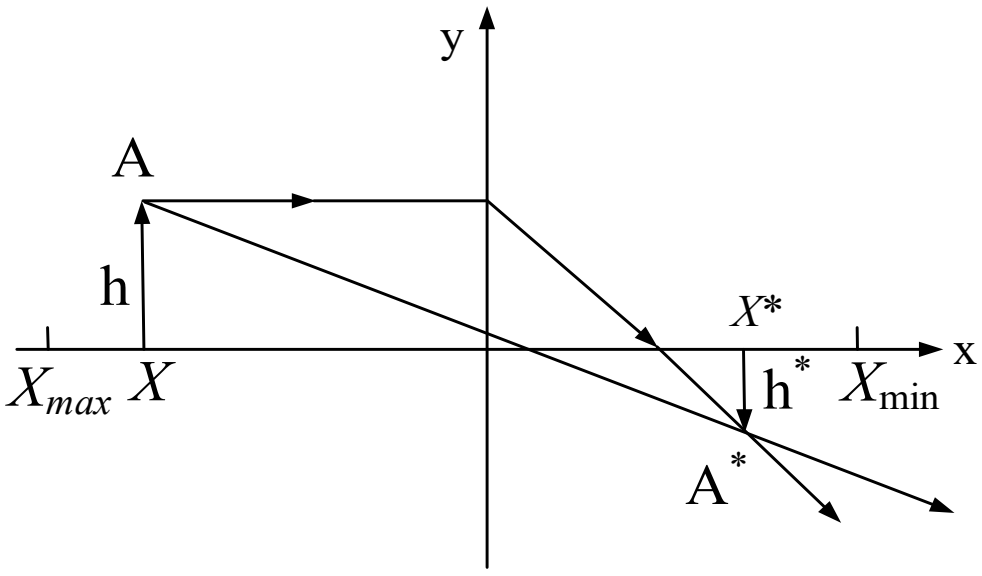


Figure 3. Principle of the Reflection Backward Learning Strategy.

The flowchart of the improved IGWO algorithm is shown Figure 4:

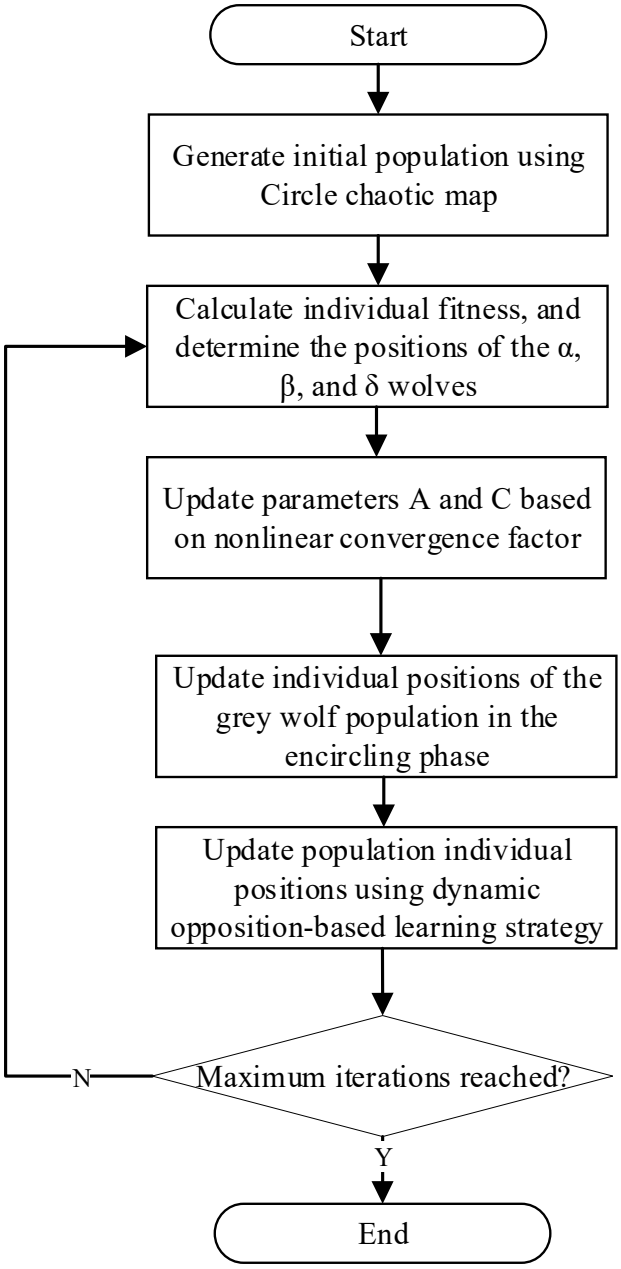


Figure 4. Improved Gray Wolf Algorithm Flowchart.

5. Experimental Results

5.1. Study Area

Shenzhen City is located in southern Guangdong Province, characterized by diverse topography and complex climatic conditions. It boasts the highest number of super high-rise buildings in China, covering an area of 1997 square kilometers. The city administers nine districts and two functional zones, with a permanent population of 17.9895 million. By 2024, Shenzhen had established 250 drone flight routes and conducted 28,000 passenger helicopter flights. This study utilizes Shenzhen's 33 vertical vertiports as research subjects to validate the effectiveness of the proposed methodology, demonstrating both research rationality and practical significance for construction guidance. The locations of the vertiports are shown in Figure 5 and Table 2:

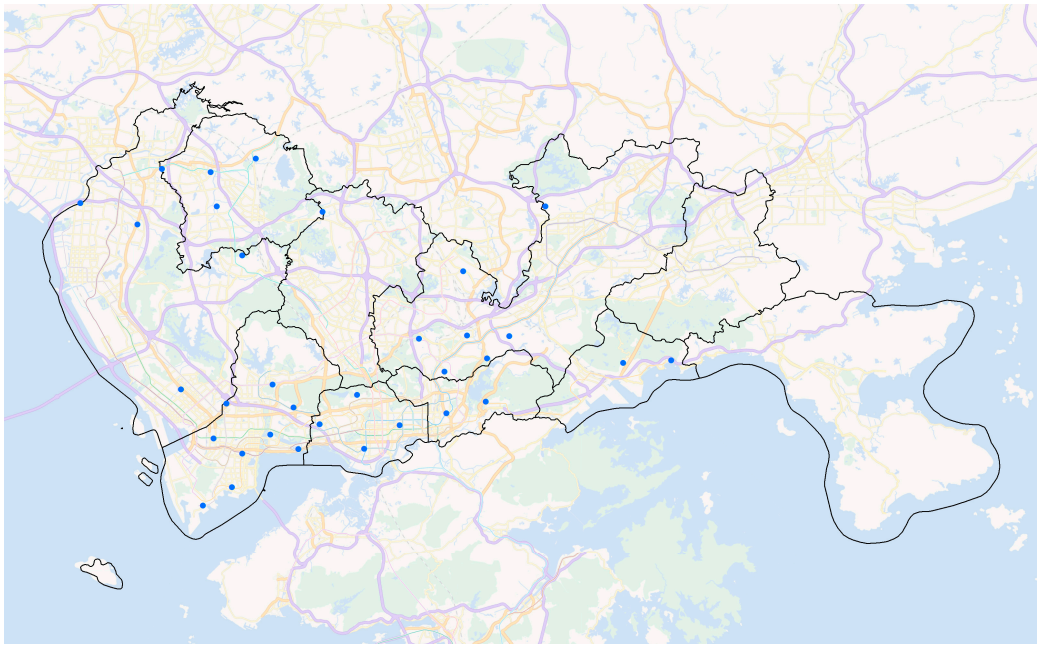


Figure 5. Location of Vertiports within the Study Area.

Table 2. WGS84 Coordinates of the Vertiport within the Study Area.

ID	Longitude	Latitude	ID	Longitude	Latitude	ID	Longitude	Latitude
0	114.0056	22.5476	11	114.2837	22.6041	22	114.2125	22.7473
1	113.9056	22.7785	12	114.1578	22.5684	23	113.9815	22.5630
2	113.9111	22.7472	13	113.9347	22.5208	24	114.1794	22.6284
3	113.9201	22.5668	14	113.9469	22.7909	25	114.1406	22.6290
4	113.9252	22.4902	15	114.0081	22.7421	26	113.9624	22.5842
5	113.8986	22.4732	16	113.8387	22.7307	27	114.0399	22.5747
6	113.9861	22.5250	17	113.9082	22.5347	28	114.137	22.6879
7	113.8609	22.7816	18	114.1199	22.5960	29	114.0788	22.5469
8	113.9603	22.5383	19	113.7863	22.7502	30	114.1218	22.5579
9	114.0965	22.6262	20	113.8783	22.5797	31	113.9345	22.7022
10	114.1590	22.6080	21	114.0463	22.5254	32	114.3276	22.6063

5.2. Calculation of Network Connectivity Distance

Given that Euclidean distance cannot accurately characterize the actual navigable distance under airspace constraints, this section calculates the actual navigable path distance between nodes using the A* algorithm, based on building data, no-fly zones, and a rasterized system, thereby providing more precise input for the network optimization model.

First, we divide the low-altitude airspace into a grid system with a 250 m resolution. Next, in accordance with the minimum safety altitude regulations in the Rules of the Air (ICAO Annex 2), aircraft flying over densely populated areas, towns, or residential areas must maintain an altitude of at least 300 m above the highest obstacle within a 600 m horizontal radius. Considering that the typical maximum flight altitude for eVTOLs is 600 m above true ground level, we set 600 m as the upper limit for flight altitude. We identified all buildings with an elevation exceeding 300 m and, for each such building, established a cylindrical flight restriction zone with a horizontal radius of 600 m and a vertical extent ranging from 300 m above the building's summit to the top of the 600 m airspace.

Regarding the no-fly zones, they were defined based on publicly available airspace classification charts and regulatory documents for the Shenzhen region. These no-fly zones

primarily include those around commercial and general aviation airports, radio facilities, and nuclear power plants, among others.

Grid cells that overlap spatially with these restricted flight zones and no-fly zones are marked as unavailable. The available airspace is shown in Figure 6.

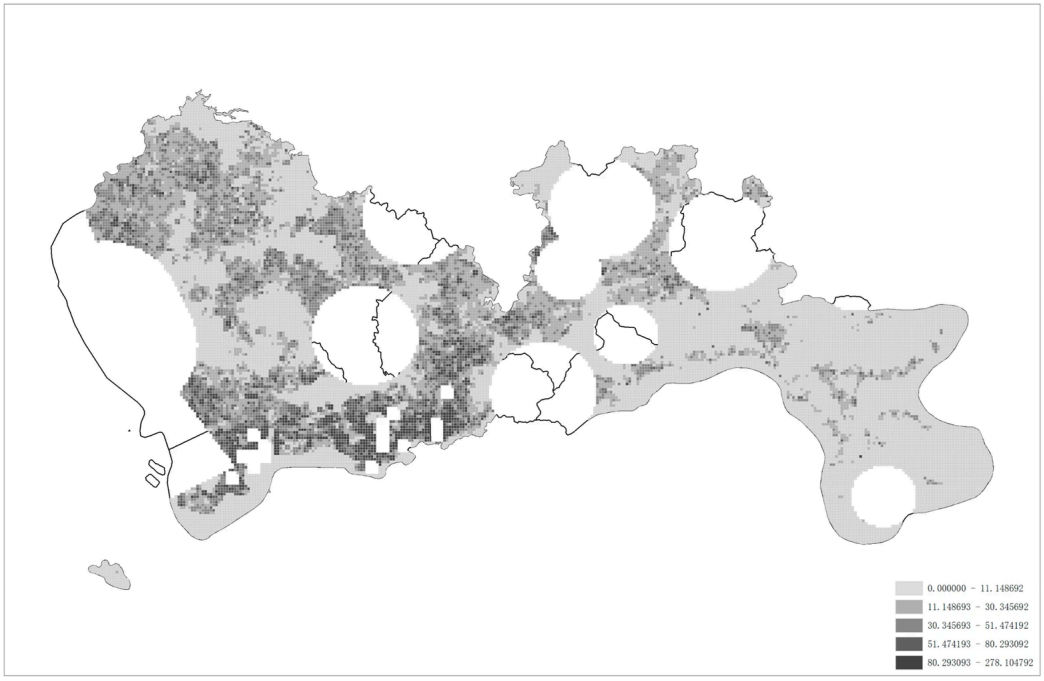


Figure 6. Available airspace grids within the study area.

After modeling the restricted airspace and obtaining a set of available airspace grids, the A* algorithm is used to search for an approximately optimal collision-free path within the free space described by the available airspace grid model, thereby determining the actual flyable path distance between any two takeoff and landing field nodes. The generated connectivity paths between vertiports are shown in Figure 7.

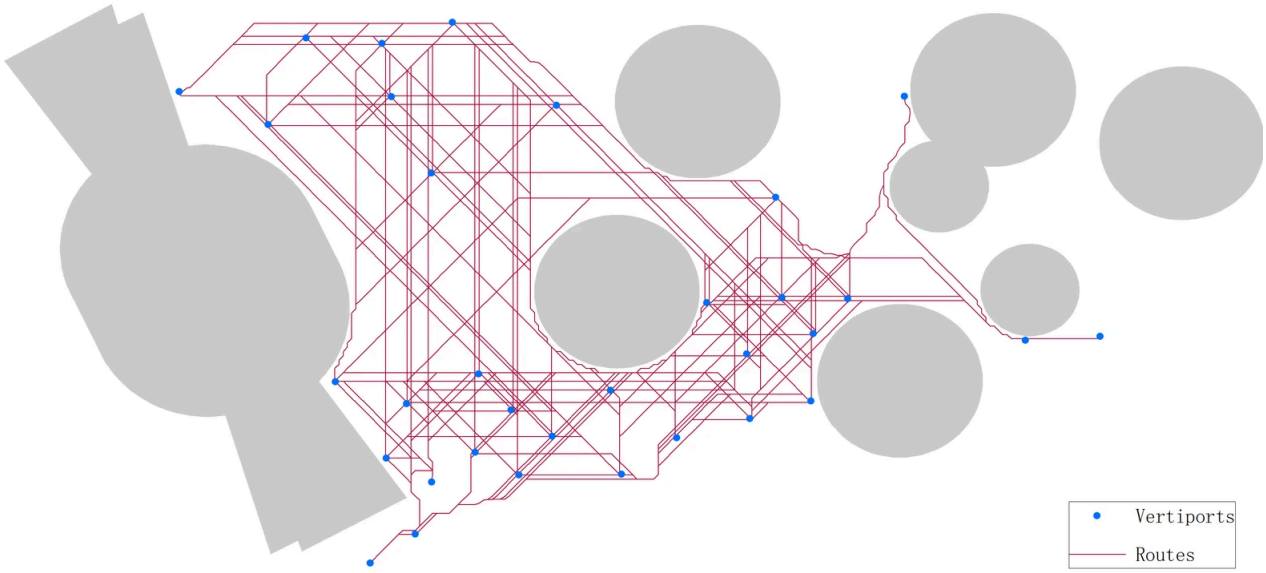


Figure 7. Connecting routes between landing and takeoff sites.

5.3. Sensitivity Analysis of Maximum Node Degree

To determine the impact of the predefined upper limit on the number of connections a single node can establish—which defines the maximum number of connections a single network node can simultaneously support in the case studies of this research—on the performance of connected networks, the maximum degree constraint K was restricted to the range 3 to 10. The IGWO algorithm was then employed to solve for the vertiports connected network with the highest normalized algebraic connectivity. The resulting network characteristics are illustrated in Figure 8.

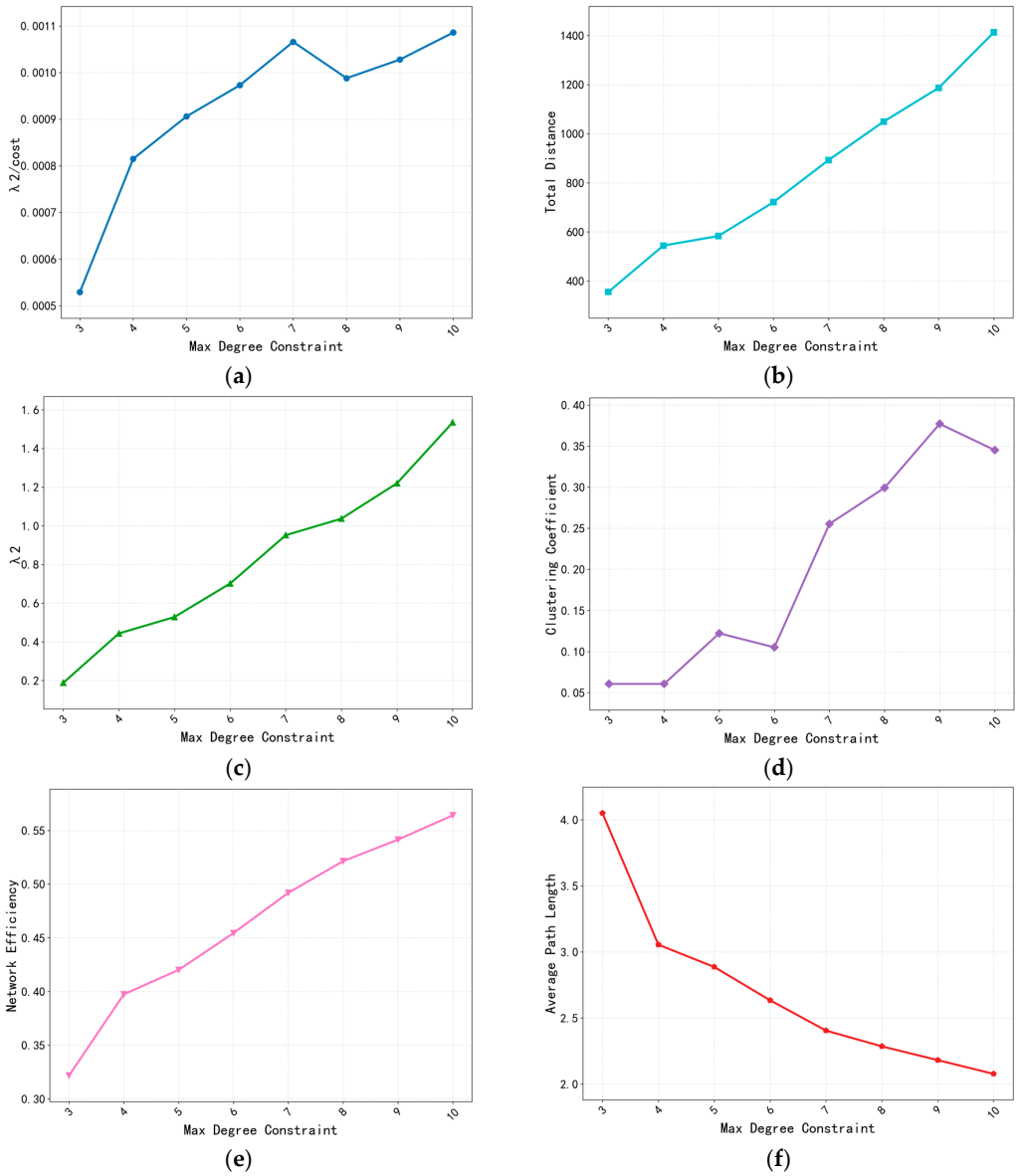


Figure 8. Network Characteristics Under Different Maximum Degree Constraints: (**a**) Objective function value; (**b**) Total Network Distance; (**c**) Algebraic Connectivity; (**d**) Aggregation coefficient; (**e**) Network Efficiency; (**f**) Average Path Length.

It can be observed that the total network distance, algebraic connectivity, network efficiency, and average path length increase or decrease in a unidirectional manner as the maximum degree constraint is increased, indicating that as the maximum degree constraint is relaxed, the network gradually becomes denser and more efficient. When K = 3, the network constraints are overly stringent, resulting in fewer edges, longer average paths, and poorer connectivity. Within the range of K = 4 to 7, both the total network distance

and network efficiency steadily improve as K increases, while the average shortest path length gradually decreases. During this phase, the algorithm tends to enhance network performance by increasing the number of edges. When K = 8, the rate of increase in total network distance exceeds the rate of improvement in algebraic connectivity, causing the objective value to decrease. When K falls within the range 9 to 10, the objective value increases again.

It can thus be concluded that the objective function performs best when the maximum degree constraint K is set to 7 or 10. A K value of 7 yields higher network efficiency, while K = 10 achieves a more optimal total network distance. The network structures when K takes the values 5, 7, and 10 are shown in Figure 9, Figure 10, and Figure 11, respectively.

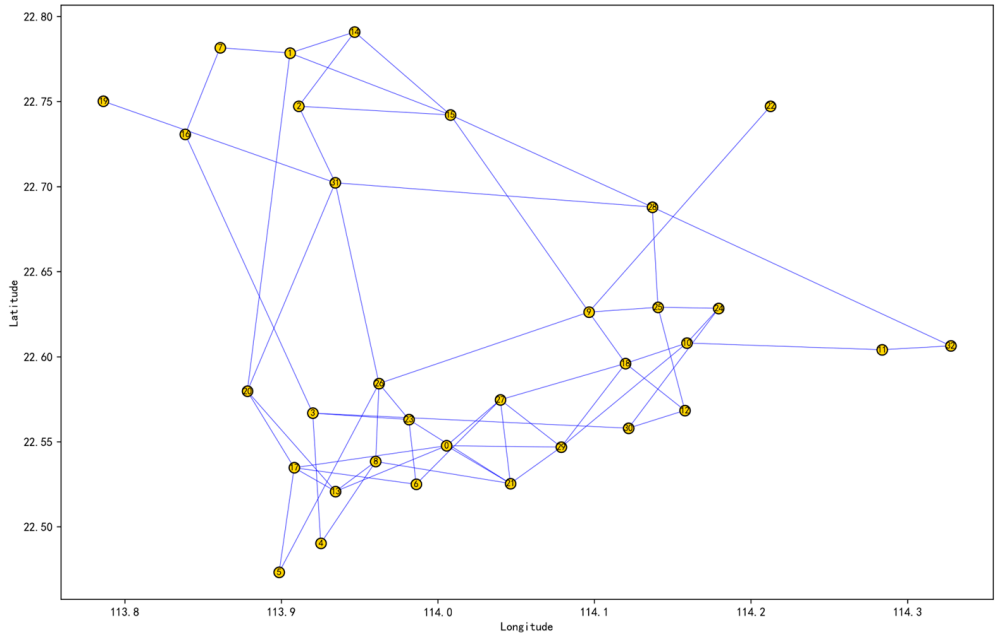


Figure 9. Connected Network of Vertiport With K = 5.

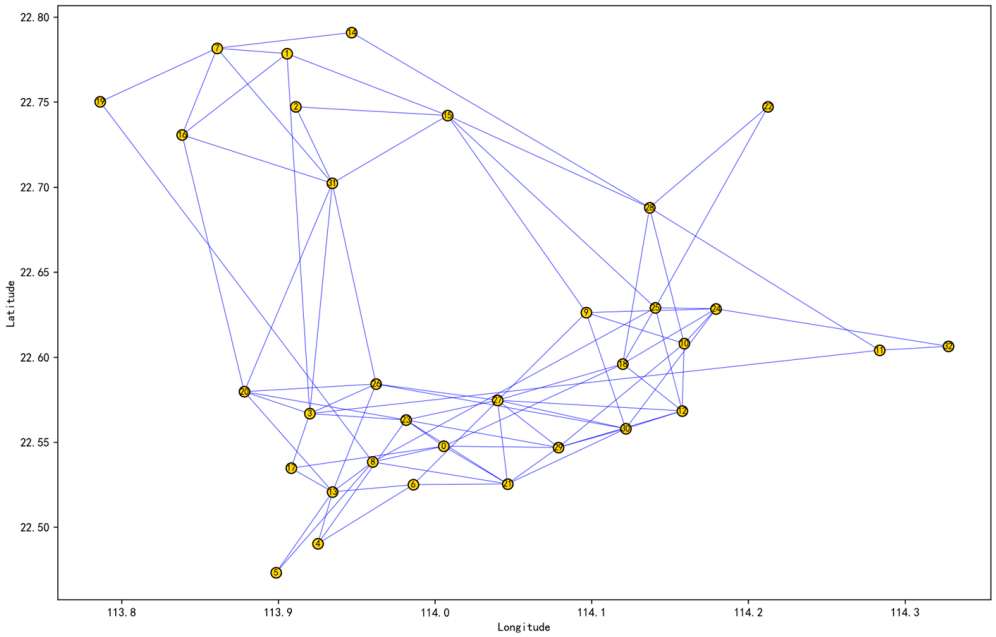


Figure 10. Connected Network of Vertiport With K = 7.

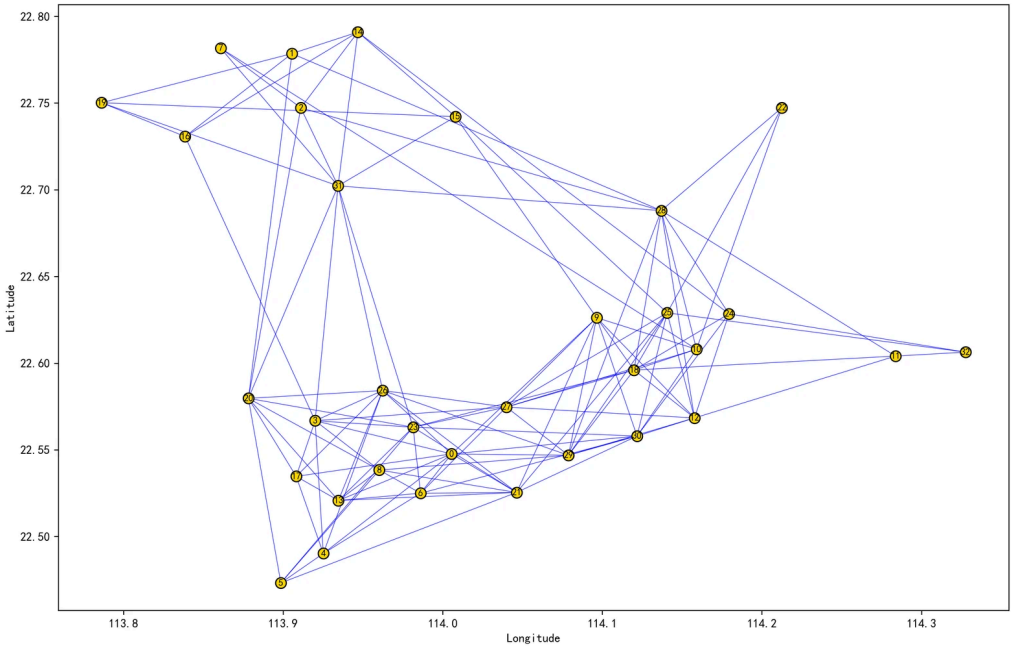


Figure 11. Connected Network of Vertiport With K = 10.

5.4. Validity Analysis

To compare the effectiveness of the low-altitude vertiport network topology constructed in this study and the capability of the IGWO algorithm in solving the vertiport network topology optimization problem, the IGWO algorithm was used alongside the standard GWO algorithm and six other heuristic algorithms to solve the problem simultaneously, enabling a comparative analysis of algorithmic performance. For model parameters, the maximum degree of nodes was set to 7. Due to current battery technology limitations, the nominal range of mainstream all-electric eVTOL aircraft used for passenger transport typically falls within the 160–250 km range. In actual operations, to ensure safety, factors such as power reserves, weather conditions, and the need for return flights or alternate landings must be taken into account. Therefore, the maximum distance $D_{\max}$ was set to 100 km. To ensure fairness in comparison, the population size for all algorithms was uniformly set to 50, with a maximum iteration count of 1000, the algorithm is considered to have converged when there is no improvement in fitness within 200 iterations. Each algorithm is run independently 20 times, and the average of the metrics is used for comparison. The values for the other parameters in these meta-heuristic algorithms are shown in Table 3.

Using the aforementioned algorithms, the connectivity network topology optimization problem—aiming for maximum normalized algebraic connectivity—was solved based on the vertiport siting plan for Shenzhen. Algorithms were implemented using Python 3.13.7 and executed on a PC equipped with an Intel® Core™ i5-14600KF CPU, 5.30 GHz, and 32.00 GB RAM. Results from each algorithm are presented in Table 4.

The experimental results show that, compared to the standard GWO algorithm, the improved IGWO algorithm designed connected networks with an average normalized algebraic connectivity of 0.000950, representing a 16.00% improvement over the traditional GWO algorithm (0.000819); λ_2 improved by 18.26% (from 0.671697 to 0.794373). These results validate the effectiveness of the improvement strategy: chaotic initialization enhances the diversity and exploratory capacity of the initial population, the nonlinear convergence factor achieves a dynamic balance between the algorithm's global search and local exploration capabilities, and the dynamic refractive back-learning mechanism effectively avoids

the shortcomings of the original GWO algorithm, such as premature convergence and getting trapped in local optima. In terms of convergence and computational performance, the IGWO algorithm converged after 484 iterations, an increase of 5.70% compared to the GWO's 308.2 iterations. The corresponding average runtime was 325.46 s, an increase of 6.13% compared to the GWO's 306.65 s. This phenomenon indicates that the IGWO algorithm does not exhibit a significant decline in solution efficiency; rather, the slight increase in the number of iterations and runtime stems from the improved algorithm retaining a more thorough global search phase during the optimization process, thereby avoiding the problem of getting stuck in local optima due to rapid convergence, which is common in traditional GWO algorithms.

Table 3. Parameter Settings for the Algorithms Used in Comparison.

Algorithm Name	Parameter Settings
GWO	Linear decreasing factor $\vec{a} \in [0, 2]$
MPA	FADs effect probability = 0.2, Switching probability p = 0.5; cognitive coefficient CI = 0.1, social coefficient SI = 0.1
BFA	Chemotactic behavior probability θ = 0.8, perception strength c = 0.1; scent concentration coefficient C = 0.01
BOA	Elite individual proportion p = 0.8, Lévy flight scaling factor a = 0.5
SSA	Safety threshold st = 0.8, discoverer proportion pd = 0.2, sentinel proportion sd = 0.1
ABC	Scout bee threshold limit = 50, employed bee proportion ER = 0.5; onlooker bee proportion OR = 0.5
AO	Global exploration coefficient G = 0.01; adaptive adjustment coefficient A = (2*iter/max_iter) + (1 − iter/max_iter)

Table 4. Comparison of Optimization Results Across Different Algorithms.

Algorithm	Objective Function	λ_2	Network Distance (km)	Edge Count	Operating Time (s)	Max Iterations
IGWO	0.000950	0.794373	836.13	81.2	325.46	484
GWO	0.000819	0.671697	820.79	84	306.65	308.2
MPA	0.000835	0.731647	873.27	86.6	257.32	333.2
SSA	0.000833	0.697335	834.93	84.6	153.18	256
ABC	0.000777	0.643436	827.82	84.6	282.24	260.8
BOA	0.00079	0.683598	863.08	90.2	221.92	219.2
AO	0.000758	0.639826	843.17	87.8	243.98	267.6
BFA	0.000729	0.621308	844.46	88	228.08	256

Compared with other meta-heuristic algorithms, the IGWO algorithm achieved the optimal values for the objective function (0.000950) and λ_2 (0.794373) among all evaluated algorithms, indicating that the networks designed by the IGWO algorithm possess stronger resistance to fragmentation. In terms of edge count, the networks constructed by IGWO had the lowest average number of edges (81.2), representing a 9.98% reduction compared to the BOA algorithm (90.2), which had the highest edge count, effectively reducing network connectivity redundancy. Regarding convergence performance, the IGWO algorithm's average number of iterations to termination and runtime were higher than those of the other evaluated algorithms; therefore, it does not offer a competitive advantage in scenarios involving real-time planning problems. For offline planning problems such as low-altitude vertiport network topology planning, solution accuracy takes precedence over real-time computational efficiency. The IGWO algorithm's improvement strategy effectively avoids

the "premature convergence" issue commonly found in meta-heuristic algorithms with an acceptable increase in iteration duration, resulting in higher-quality optimization outcomes. The iterative processes of different algorithms are illustrated in Figure 12.

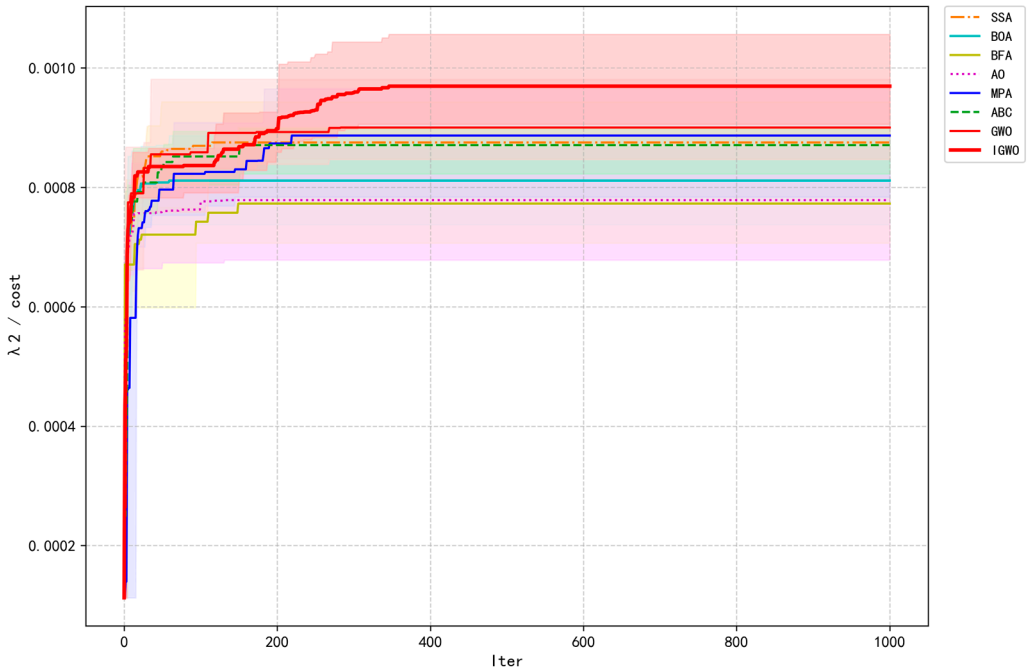


Figure 12. Iteration Curves for Different Algorithms.

To further validate the algorithm's performance, we use the SDP relaxation method to quantify the theoretical upper bound of the solution to the original problem, thereby demonstrating the degree of convergence between the algorithm's results and the global optimal solution. The relative Gap between the objective value and the theoretical upper bound is calculated as follows:

$$Gap = \frac{\alpha^*{}_{SDP} - f_{alg}}{\alpha^*{}_{SDP}} \tag{19}$$

where $\alpha^*{}_{SDP}$ is the theoretical upper bound obtained by relaxing the original problem via SDP; f_{alg} is the solution obtained by the meta-heuristic algorithm.

According to Equations (1)–(10), the theoretical upper bound $\alpha^*{}_{SDP}$ of the objective function for the original problem is 0.001182, with a relative gap of 10.66% compared to the optimal value (0.001056) obtained by the IGWO algorithm. Since the upper bound of the SDP is the theoretical optimal value of the original problem under continuous relaxation, which allows the edge to take any continuous value in the interval $[0, t]$, it is possible to construct an ideal Laplacian matrix eigenvalue distribution that cannot be achieved under discrete topologies. The feasible solution obtained by the IGWO algorithm under discrete multi-constraint topology retains 89.34% of the theoretically optimal normalized algebraic connectivity, verifying the algorithm's feasibility in solving NP-hard combinatorial optimization problems.

In summary, for the high-dimensional, non-convex combinatorial optimization problem of optimizing the resilience of low-altitude takeoff and landing site network topologies, the IGWO algorithm employed in this paper demonstrates strong global optimization capabilities. It accurately identifies and prioritizes the construction of key connecting edges that contribute most significantly to the network's overall resilience, thereby avoiding the

inefficient accumulation of redundant edges in the network and achieving the planning objectives of low investment and high resilience.

5.5. Network Topology Analysis

To further analyze the properties of the vertiport network topology, the distributions of degree centrality and betweenness centrality for nodes in a connected network with K = 7 were statistically examined. The statistical results are shown in Figure 13.

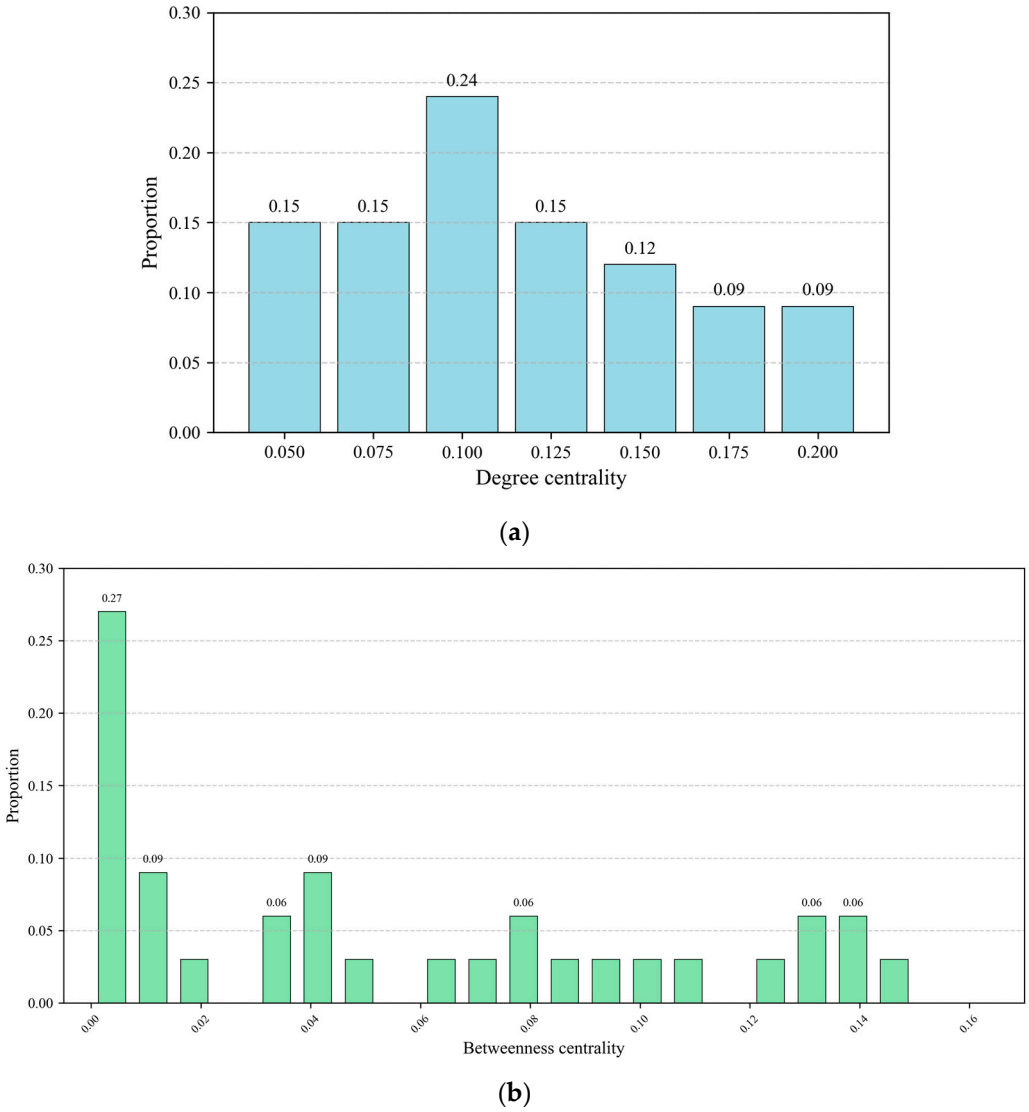


Figure 13. Network Feature Distribution: (**a**) Node Degree Centrality; (**b**) Node Betweenness Centrality.

It can be observed that the degree centrality of nodes is relatively balanced. Approximately 24% of nodes exhibit degree centrality clustered around 0.10, while the proportion of nodes in other centrality intervals is distributed within the range [0.05, 0.15]. Furthermore, no nodes in the network display degree centrality significantly exceeding 0.20. This indicates the absence of highly connected hub nodes with concentrated resources within the network. Regarding the degree centrality distribution of nodes, 27% of nodes are end nodes with zero-degree centrality. The remaining nodes exhibit relatively dispersed degree centrality, indicating that relay functions are distributed relatively evenly across multiple nodes. Based on the above analysis, this network exhibits decentralized characteristics, with most nodes possessing a similar number of connections. This dispersed structure

effectively mitigates the risk of widespread network failure caused by the failure of a single critical node, thereby enhancing network resilience and fairness.

5.6. Resiliency Analysis of Vertiport Network Topology

Resilience analysis evaluates a network's ability to maintain connectivity, efficiency, and functional integrity when fragmented due to partial node or edge failures. Consequently, attack strategies determine the sequence and severity of node or edge failures under perturbations. When studying network resilience, two forms of disruption are typically considered: random attacks and malicious attacks.

The random attack model simulates natural equipment aging, severe weather, or sporadic failures. It involves randomly causing a certain proportion of nodes or edges in the network to fail with a certain probability, without taking into account the network's characteristics or nature. Individual random failure events are unpredictable, and their effects are typically localized and gradual; unless they accumulate to a certain extent, they are unlikely to cause a complete system failure.

The deliberate attack mode simulates malicious sabotage, overload caused by high traffic, or other forms of targeted network destruction. Attackers leverage their knowledge of the network to actively and strategically damage it, aiming to maximize the destructive impact. Common attack strategies include dynamic maximum degree attacks, which target the node or edge with the highest number of connections and, after its failure, sequentially identify the node or edge with the highest degree in the current network; and dynamic maximum betweenness attacks, which target the most critical node or edge in all shortest paths and, after its failure, sequentially identify the node or edge with the highest betweenness in the current network. Malicious attacks can effectively disrupt information flow within a network, often triggering cascading failures and inflicting rapid and devastating damage on the network.

In this study, five attack patterns are employed to analyze the performance of the vertiport connectivity network under these disruptions: random node failure, random edge failure, malicious attacks based on node degree ranking, malicious attacks based on node betweenness centrality ranking, and malicious attacks based on edge betweenness centrality ranking. To quantify network resilience, the Giant Component Ratio (GCR) and global network efficiency are employed as evaluation metrics for topological resilience.

GCR quantifies the proportion of the largest connected component in the remaining network after disruption relative to the original network, reflecting the degree of network fragmentation.

$$GCR = \frac{N'}{N} \tag{20}$$

where N' denotes the number of nodes contained in the largest connected subgraph within the remaining portion of the network after it has suffered an attack or experienced a failure.

Global Network Efficiency (E_G) measures the efficiency of communication between nodes within a network. Typically, the average shortest path length $\overline{L}$ indicates connectivity convenience between nodes. However, network resilience analysis faces a challenge: when no path connects two nodes, their distance is treated as infinite. This causes the metric to fail when the network splits into two disconnected subgraphs. Global network efficiency employs the reciprocal of the shortest path distance, thereby circumventing the issue of uncomputable metrics during network disruptions.

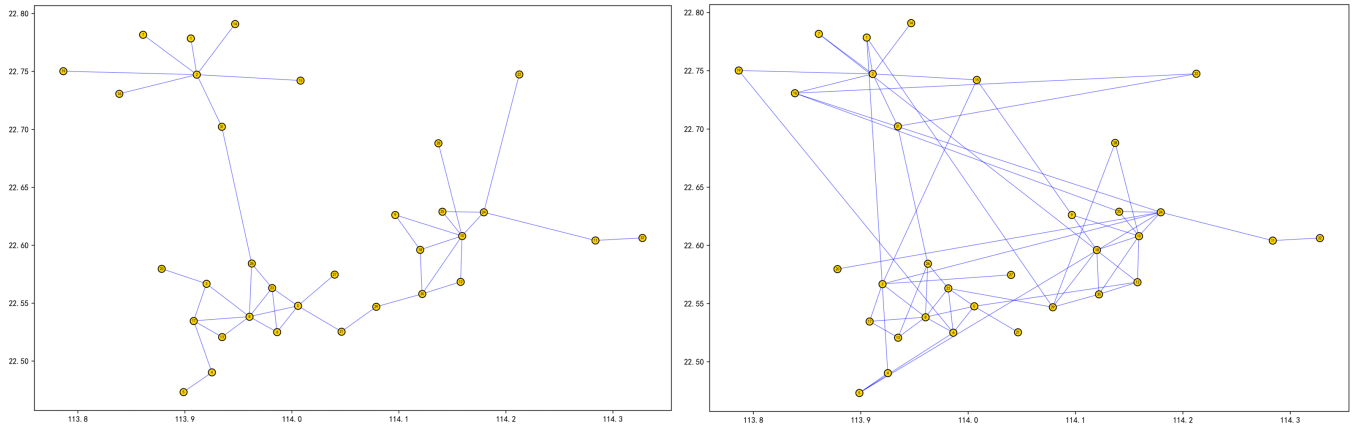
$$E_G = \frac{1}{N(N-1)} \sum_{i \neq j} \frac{1}{D_{ij}} \ \forall v_i, v_j \in V \tag{21}$$

where D_{ij} is the shortest path distance between nodes v_i and v_j.

The GCR and E_G metrics reflect a network's ability to maintain structural integrity under disruption, making them widely used in network resilience analysis.

5.6.1. Comparison of the Robustness Under Random Attacks

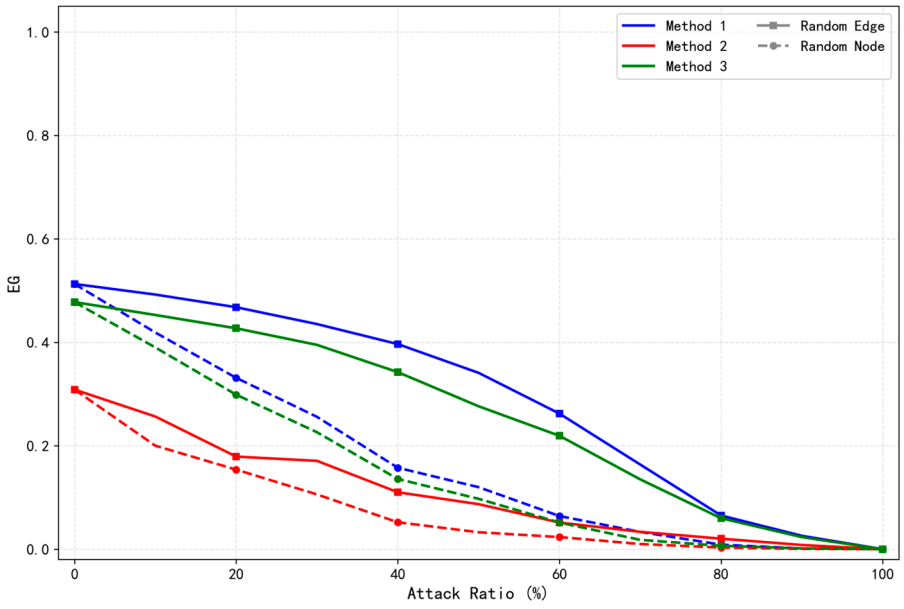
To more intuitively demonstrate the resilience of the low-altitude vertiport network topology constructed in this paper, this section constructs vertiport networks based on both a hub-and-spoke network model and a hybrid network model that protects critical nodes by adding edges. These networks are used to compare the resilience levels with those of the network constructed by the model that aims for maximum algebraic connectivity [20,21]. The networks constructed using these two network models in this case study are shown in Figure 14.



(**a**) (**b**)

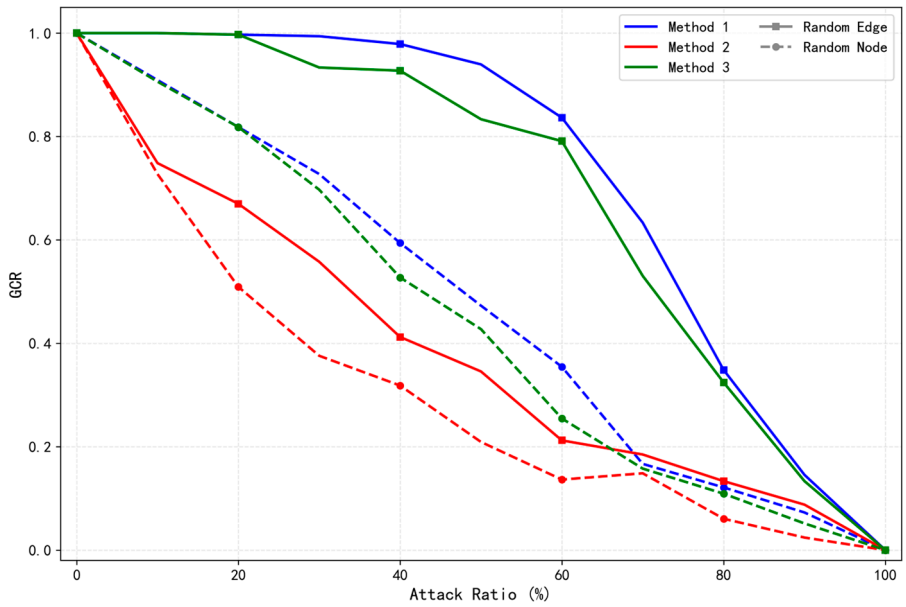
Figure 14. Network Model for Comparing Resilience: (**a**) Hub-and-poke; (**b**) hybrid.

Figure 15 illustrates the changes in GCR and E_G for the vertiport network generated using three network models under random attacks.



(**a**)

Figure 15. *Cont.*



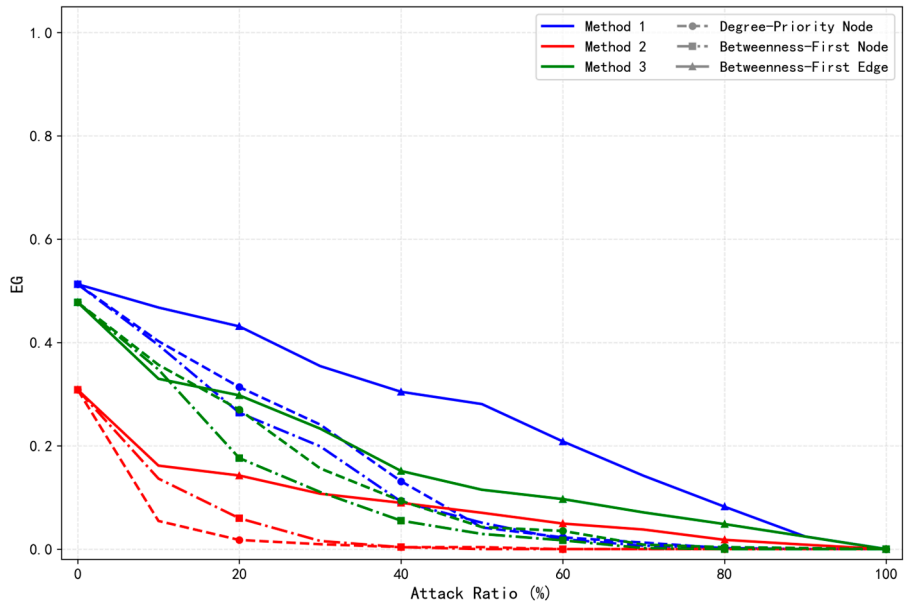
(**b**)

Figure 15. Network Resilience Under Random Attacks: (**a**) *GCR*; (**b**) E_G.

It can be observed that the network constructed using this research methodology outperforms the comparison network in both the proportion of maximum connected subgraphs and overall efficiency under random node attacks and random edge attacks. Even when the attack ratio reaches 60%, the network maintains good connectivity and efficiency. This demonstrates that the topological network exhibits high stability during daily operations, reducing the impact of equipment failures and unexpected events on the service level of the transportation network.

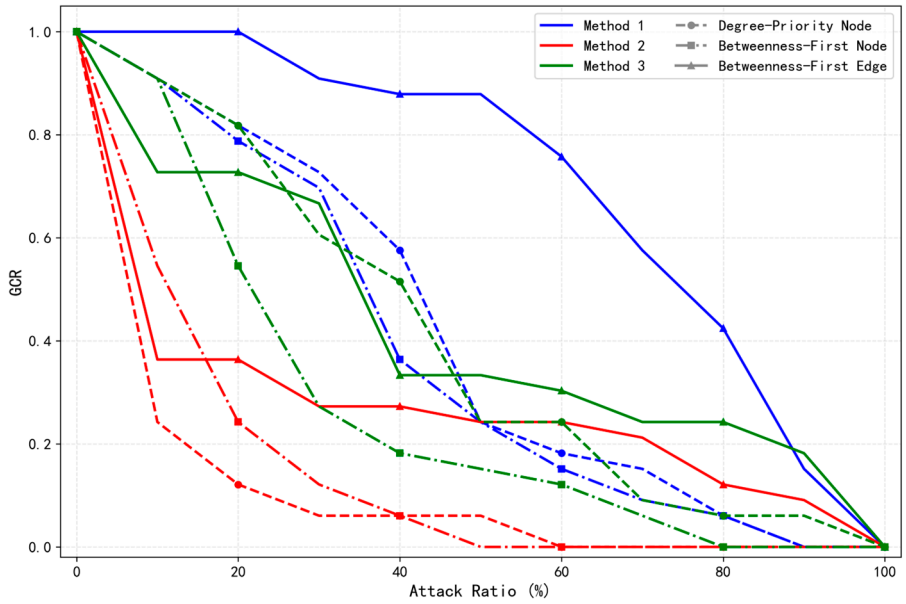
5.6.2. Comparison of the Robustness Under Deliberate Attack

Under deliberate attack scenarios, the *GCR* and E_G changes for the vertiport network generated using three network models are shown in Figure 16.



(**a**)

Figure 16. *Cont.*



(**b**)

Figure 16. Network Resilience Under Deliberate Attacks: (**a**) GCR; (**b**) E_G.

It can be observed that under all malicious attack scenarios, the global efficiency of the vertiport connectivity network constructed using the method proposed in this study consistently achieves optimal performance, outperforming both the hub-and-spoke network and the hybrid network. In terms of the proportion of the maximum connected subgraph, the network constructed by the model proposed in this study performs similarly to the hybrid network model under degree-priority node attacks; under degree-first node attacks, it performs slightly better than the hybrid network; and under degree-first edge attacks, it significantly outperforms other networks. This indicates that the low-altitude vertiport connectivity network constructed by the model proposed in this paper can effectively cope with connectivity disruptions between vertiport nodes while also demonstrating good resilience against node failures. Overall, the network constructed in this study performs well under most threat scenarios, demonstrating inherent security and reliability.

6. Conclusions

This study investigates the optimization of topological resilience for low-altitude vertiport networks, establishing a network modeling and optimization method that balances resilience performance with economic feasibility. The core theoretical contribution lies in successfully shifting the network resilience optimization problem from the traditional "maximization of algebraic connectivity" paradigm to the "maximization of normalized algebraic connectivity" paradigm. Its profound significance lies in embedding the multi-dimensional trade-off between resilience and cost into a single-objective optimization model. This approach identifies and prioritizes critical connections that significantly enhance overall resilience while maintaining relatively low construction costs. As a result, it avoids redundant investments that are difficult to sustain in real-world scenarios. This optimization philosophy holds significant practical guidance value for planning low-altitude infrastructure networks, which are characterized by high construction costs and limited airspace resources.

The core theoretical contribution of this study lies in shifting the objective of network fault tolerance optimization from the traditional "maximizing algebraic connectivity" paradigm to the "maximizing normalized algebraic connectivity" paradigm. This transformation achieves an effective trade-off between fault tolerance and construction costs. In

addition, it embeds multi-dimensional optimization objectives into a single-objective model through objective function design, thereby improving the model's engineering applicability. Specifically, the proposed method intelligently identifies and prioritizes the construction of critical connections that significantly contribute to global resilience while incurring lower construction costs. This approach substantially enhances network robustness while controlling the total network distance. For instance, experimental results demonstrate that under identical constraints, the network generated by the IGWO algorithm achieved an average normalized algebraic connectivity that was 16.00% higher than that of the traditional GWO algorithm across 20 repeated experiments. In resilience analysis, simulations of five node and edge failure modes reveal that the constructed network significantly outperforms both hub-and-spoke and hybrid networks in terms of maximum connected subgraph proportion and global efficiency. Particularly under random attacks and degree-based targeted attacks, the network maintained high connectivity even with 60% node or edge failures, demonstrating robust inherent resilience and engineering applicability.

Although this study advances fault-tolerant optimization for low-altitude vertiport networks, several limitations remain, pointing to future research directions:

First, the model does not account for node or edge performance degradation or dynamic fault propagation. In real-world low-altitude traffic networks, vertiports may experience reduced throughput efficiency due to traffic saturation. Future work could incorporate node capacity constraints and dynamic edge weights (e.g., transit time, traffic volume) to more accurately reflect the network's operational dynamics. The resilience analysis in this study primarily focuses on static topologies. Subsequent work could incorporate dynamic load redistribution models and geographic block attack simulations to further enrich the dimensions of network resilience assessment.

Second, the model projects three-dimensional airspace problems onto a two-dimensional plane and simplifies flight path costs using straight-line distances. This approach overlooks essential factors in real low-altitude flight, such as three-dimensional trajectory planning, terrain avoidance, and building obstacle avoidance. For instance, vertiports atop high-rise buildings may have short straight-line distances but require complex ascents and detours in actual flight paths. Therefore, integrating 3D Geographic Information Systems (3D-GIS) with airspace obstacle models to construct cost models closer to real-world flight environments is a key direction for enhancing the engineering feasibility of the solution.

Finally, while the improved IGWO algorithm demonstrated excellent performance in the 33-vertiport case study, its efficiency and stability for solving larger-scale networks (e.g., hundreds of nodes covering the Guangdong-Hong Kong-Macao Greater Bay Area) require further validation. Future research may explore combining distributed parallel computing frameworks with meta-heuristic algorithms or employing community detection-based problem decomposition strategies to overcome computational bottlenecks in ultra-large-scale combinatorial optimization problems.

In summary, this study provides theoretical foundations and methodological support for resilience-optimized low-altitude vertiport networks. The proposed model and algorithm significantly enhance network resilience while maintaining cost control. Future research will delve deeper into three-dimensional environment modeling, dynamic operational constraints, and large-scale solution approaches, propelling low-altitude transportation networks from static topology design toward dynamic intelligent planning.

Author Contributions: Conceptualization, H.X. and J.Y.; methodology, J.Y. and Z.Z.; software, L.Z.; validation, H.X. and J.Y.; formal analysis, Y.W.; investigation, Z.Z.; resources, J.Y.; data curation, Q.W.; writing—original draft preparation, H.X.; writing—review and editing, H.X. and J.Y.; visualization, L.Z.; supervision, J.Y.; project administration, J.Y. All authors have read and agreed to the published version of the manuscript.

Funding: This research was funded by the Frontier Technology R&D Program of Jiangsu Province (No. BF2025009), the Major Science and Technology Project of Jiangsu Province (No. BG2025007), the Major Science and Technology Project of Nanjing (No. 202405026), the Shenzhen Natural Science Foundation in Basic Research Fund (No. JCYJ20250604190030038), and the Shenzhen Longhua Science and Technology Innovation Special Funding Project (Industrial Sci-Tech Innovation Center of Low-Altitude Intelligent Networking).

Institutional Review Board Statement: Not applicable.

Informed Consent Statement: Not applicable.

Data Availability Statement: Data are contained within the article.

Conflicts of Interest: Author Long Zhou was employed by the company Nanjing Intelligent Aviation Research Institute Co., Ltd. The remaining authors declare that the research was conducted in the absence of any commercial or financial relationships that could be construed as a potential conflict of interest.

Abbreviations

The following abbreviations are used in this manuscript:

GWO	Global Wolf Pack Optimization
eVTOL	Electric Vertical Take-off and Landing
UAM	Urban Air Mobility
DDoS	Distributed Denial of Service
UMT	Urban Multi-Modal Transportation
MST	Minimum Spanning Tree
SDP	Semi-Definite Programming
GCR	Giant Component Ratio
3D-GIS	Three-Dimensional Geographic Information Systems

References

1. Lieberthal, E.B.; Serok, N.; Duan, J.; Zeng, G.; Havlin, S. Addressing the urban congestion challenge based on traffic bottlenecks. *Philos. Trans. A* **2024**, *382*, 20240095. [CrossRef] [PubMed]
2. Louzada, V.H.; Daolio, F.; Herrmann, H.J.; Tomassini, M. Smart rewiring for network robustness. *J. Complex Netw.* **2013**, *1*, 150–159. [CrossRef]
3. Mahabadi, Z.; Varga, L.; Dolan, T. Network properties for robust multilayer infrastructure systems: A percolation theory review. *IEEE Access* **2021**, *9*, 135755–135773. [CrossRef]
4. Calvert, S.C.; Snelder, M. A methodology for road traffic resilience analysis and review of related concepts. *Transp. A Transp. Sci.* **2018**, *14*, 130–154. [CrossRef]
5. Chung, S.; Sardak, D.; Cegan, J.; Linkov, I. Assessing the Robustness and Resilience of US Strategic Highways: A Network Science Perspective. *Transp. Res. Rec.* **2025**, *2679*, 480–495. [CrossRef]
6. Ren, G.; Liu, Y. Modeling and Invulnerability Analysis of Multilayer Air Traffic Network considering Altitude Layer. *Int. J. Aerosp. Eng.* **2023**, *2023*, 6525201. [CrossRef]
7. Lu, M.; Perez, E.J.; Mason, K. Complex network analysis of China's integrated air-high-speed rail network: Topological characteristics, centrality measures, and cluster analysis. *J. Transp. Geogr.* **2025**, *127*, 104292. [CrossRef]
8. Morfin Veytia, A.; Ellerbroek, J.; Hoekstra, J. Decentralised Traffic Management for Constrained Urban Airspace: Dynamically Generating and Acting Upon Aggregate Flow Data. *J. Open Aviat. Sci.* **2024**, *2*.
9. Clarke, S.G.; Hwang, S.; Thapliyal, O.; Hwang, I. Distributed Denial-of-Service Resilient Control for Urban Air Mobility Applications. *J. Aerosp. Inf. Syst.* **2023**, *20*, 873–889. [CrossRef]
10. Ma, Z.; Yang, X.; Chen, A.; Zhu, T.; Wu, J. Assessing the resilience of multi-modal transportation networks with the integration of urban air mobility. *Transp. Res. Part A Policy Pract.* **2025**, *195*, 104465. [CrossRef]
11. Ma, Z.; Wang, Z.; Peng, Y.; Xu, Y.; Chen, A.; Yang, X.; Wu, J. Equity analysis of urban transportation network resilience with urban air mobility integration. *Case Stud. Transp. Policy* **2025**, *23*, 101673. [CrossRef]
12. Zhang, W.; Hwang, T. UAM Vertiport Network Design Considering Connectivity. *Systems* **2025**, *13*, 607. [CrossRef]

13. Song, K.-H.; Lee, H. Network topology-driven vertiport placement strategy: Integrating urban air mobility with the Seoul Metropolitan railway system. *Appl. Sci.* **2025**, *15*, 3965. [CrossRef]
14. Fung, T.-Y. Designing Resilient Urban Air Mobility Systems Through Simulation of Off-Nominal Disruptions. Doctoral Dissertation, Purdue University, Lafayette, Indiana, 2025.
15. Liu, J.; Zhu, G.; Yang, L.; Shen, Y. Suitability assessment and route network planning for low-altitude transportation in urban agglomerations using multi-source data. *Aerospace* **2025**, *12*, 777. [CrossRef]
16. Cheng, M.; Huang, H. Analysis of the Impact of Weather on the Robustness of Low-Altitude Route Networks. *J. Transp. Syst. Eng. Inf. Technol.* **2025**, *25*, 101–108+275.
17. Kim, Y.; Mesbahi, M. On maximizing the second smallest eigenvalue of a state-dependent graph Laplacian. In Proceedings of the 2005, American Control Conference, 2005, Portland, OR, USA, 8–10 June 2005; pp. 99–103.
18. Mosk-Aoyama, D. Maximum algebraic connectivity augmentation is NP-hard. *Oper. Res. Lett.* **2008**, *36*, 677–679. [CrossRef]
19. Long, W.; Wu, T.; Cai, S.; Liang, X.; Jiao, J.; Xu, M. A novel grey wolf optimizer algorithm with refraction learning. *IEEE Access* **2019**, *7*, 57805–57819. [CrossRef]
20. Willey, L.C.; Salmon, J.L. A method for urban air mobility network design using hub location and subgraph isomorphism. *Transp. Res. Part C Emerg. Technol.* **2021**, *125*, 102997. [CrossRef]
21. Tomassini, M. Rewiring or adding links: A real-world case study of network vulnerability. *Phys. A Stat. Mech. Its Appl.* **2023**, *630*, 129241. [CrossRef]

Disclaimer/Publisher's Note: The statements, opinions and data contained in all publications are solely those of the individual author(s) and contributor(s) and not of MDPI and/or the editor(s). MDPI and/or the editor(s) disclaim responsibility for any injury to people or property resulting from any ideas, methods, instructions or products referred to in the content.